# REPORT DOCUMENTATION PAGE

Form Approved
OBM No. 0704-0188



| 2. Report Date. | 3. Report Type and Dates Covered. |
|---|---|
| January 1993 | Final - Journal Article |

**4. Title and Subtitle.**
Fine Structure of Methand Hydrate-Bearing Sediments on the Blake Outer Ridge as Determined From Deep-Tow Multichannel Seismic Data

**5. Funding Numbers**

| | |
|---|---|
| Contract | |
| Program Element No | 0602435N |
| Project No | 03502 |
| Task No | JOB |
| Accession No | DN259007 |
| Work Unit No | 13620H |

**6. Author(s).**
M. M. Rowe and J. F. Gettrust



**7. Performing Organization Name(s) and Address(es).**
Naval Research Laboratory
Ocean Science Directorate
Stennis Space Center, MS 39529-5004

**8. Performing Organization Report Number.**
JA 362:072:91

**9. Sponsoring/Monitoring Agency Name(s) and Address(es).**
Naval Research Laboratory
Ocean Acoustics and Technology Directorate
Stennis Space Center, MS 39529-5004

**10. Sponsoring/Monitoring Agency Report Number.**
JA 362:072:91

**11. Supplementary Notes.**
Published in Journal of Geophysical Research.

**12a. Distribution/Availability Statement.**
Approved for public release; distribution is unlimited.

**12b. Distribution Code.**

**13. Abstract** *(Maximum 200 words).*

High-resolution, deep-tow multichannel seismic data are used to investigate the detailed structure of sediments containing methane hydrate. These data support thick, laterally extensive layers of methane hydrate-bearing sediment underlain by a bottom simulating reflector (BSR) and spatially discontinuous zones of hydrate within the sediments above the BSR depth where no BSR is present. These data resolve normal faults which extend from the surface through the BSR with apparent offsets of up to 20 m. A phase inversion identified at the top of the BSR shows that the material immediately beneath the BSR has anomalously low velocity, consistent with a layer of sediment containing free methane gas. The fault offsets along the BSR and consistent with a pressure change of ~200 kPa (~2 bars) across the fault zone.



**14. Subject Terms.**
Directional ambient noise, bottom scattering, Deep-TowedAarray Geophysical System towed array, ocean-bottom seismometer

**15. Number of Pages.**
11

**16. Price Code.**

| 17. Security Classification of Report. | 18. Security Classification of This Page. | 19. Security Classification of Abstract. | 20. Limitation of Abstract. |
|---|---|---|---|
| Unclassified | Unclassified | Unclassified | SAR |

JOURNAL OF GEOPHYSICAL RESEARCH, VOL. 98, NO. B1, PAGES 463–473, JANUARY 10, 1993

# Fine Structure of Methane Hydrate-Bearing Sediments on the Blake Outer Ridge as Determined From Deep-Tow Multichannel Seismic Data

M. M. ROWE AND J. F. GETTRUST

*Naval Research Laboratory, Stennis Space Center, Mississippi*

High-resolution, deep-tow multichannel seismic data are used to investigate the detailed structure of sediments containing methane hydrate. These data support thick, laterally extensive layers of methane hydrate-bearing sediment underlain by a bottom simulating reflector (BSR) and spatially discontinuous zones of hydrate within the sediments above the BSR depth where no BSR is present. These data resolve normal faults which extend from the surface through the BSR with apparent offsets of up to 20 m. A phase inversion identified at the top of the BSR shows that the material immediately beneath the BSR has anomalously low velocity, consistent with a layer of sediment containing free methane gas. The fault offsets along the BSR are consistent with a pressure change of ~200 kPa (~2 bars) across the fault zone.

## INTRODUCTION

In 1989 the Naval Oceanographic and Atmospheric Research Laboratory, now part of the Naval Research Laboratory (NRL), conducted a deep-tow multichannel seismic study on the Blake Outer Ridge (Figure 1) that included profiles to resolve the detailed structure of methane hydrates which have been identified in that region [*Shipley et al.*, 1979; *Paull and Dillon*, 1981; *Markl and Bryan*, 1983]. The detailed vertical and lateral distribution of gas hydrates has been difficult to assess because the hydrate is stable only within the upper sediments (to 800 m) in relatively deep water (3000 to 3600 m in this region) and are usually identified indirectly through association with a bottom simulating reflector (BSR). The BSR is a high-amplitude reflection horizon that follows seafloor topography and is thought to be the reflection from the interface between hydrate-bearing sediments at the base of the hydrate stability zone and gas-saturated sediments beneath them [*Bryan*, 1974; *Shipley et al.*, 1979; *Dillon et al.*, 1980; *Paull and Dillon*, 1981].

Gas hydrate is a specific type of clathrate, a crystalline cage structure, found in deep ocean sediments which consists of a solid lattice of water molecules in which each "cage" within the lattice encloses a gas molecule [*Sloan*, 1990]. Approximately 98% of the gas making up the hydrate in the ocean bottom is methane [*Hollister et al.*, 1972; *McIver*, 1974; *Kvenvolden and McDonald*, 1985]. The methane hydrate buried in marine sediment contains high concentrations of methane contained in the hydrate structure (as much as 170 $m^3$ of methane gas in 1 $m^3$ of methane hydrate [*Baker*, 1974; *Kvenvolden and Barnard*, 1983*a*]). In addition, large amounts of free (undissolved) methane are believed to exist trapped at the base of the methane hydrate stability zone [*Claypool and Kaplan*, 1974; *Dillon et al.*, 1980]. This trapped methane may present a significant hazard to drilling [*Miller et al.*, 1991].

Methane hydrate-bearing sediments have distinctive physical properties which differentiate them from water- or gas-saturated sediments. Compressional velocities from 2.0 to 3.8 km/s have been measured in situ using sonobuoys in drill hole measurements, and in laboratory samples of methane hydrate-saturated sediment [*Stoll et al.*, 1971; *Bryan*, 1974; *Kvenvolden and McDonald*, 1985; *Mathews and von Huene*, 1985]. Previous studies of methane hydrate-bearing marine sediments have shown that the methane hydrate may occur as a solid mass, as a filling in fractures and pore spaces, or as thin lenses within the sediment [*Brooks et al.*, 1983; *Mathews and von Huene*, 1985], and it may coexist with methane dissolved in pore fluids at variable depths within the methane hydrate stability zone [*Lancelot and Ewing*, 1972]. The zone of hydrated sediments may be thin, limited to the base of the hydrate stability zone or may extend from the base of the stability zone to the top of the sediment column [*MacLeod*, 1982].

The deep-tow geometry, source and receiver ~350 m above the seafloor (Figure 2), and high-frequency (250–650 Hz) source signal used for this study allow us to resolve sediment structural details <5 m in thickness within the upper 600–700 m of sediments. Lateral resolution of sediment structure of ~21 m is achievable using single-channel seismic sections (i.e., sections composed of a single, common offset trace from each shot gather). The seismic lines recorded by NRL's Deep-Towed Acoustics/Geophysics System (DTAGS) are on the western flank of the Blake Outer Ridge, at 29°50'N latitude, 75°35'W longitude, 135–165 km west of Deep Sea Drilling Project (DSDP) sites 102, 103, 104, and 533 (Figure 1). This region is on the southwestern margin of the area in which a BSR has been observed in seismic sections by *Paull and Dillon* [1981] and *Markl and Bryan* [1983].

The data presented here show that the compressional velocities within the upper ~650 m of sediment are appropriate for materials containing methane hydrate, though these regions are not necessarily associated with a BSR. However, the features diagnostic of methane hydrate-bearing sediment resolved with these seismic data occur in laterally and vertically discontinuous regions that appear to be larger and closer together where a BSR is observed.

## DEEP-TOW SEISMIC DATA

DTAGS multichannel seismic system (Figure 2) consists of a Helmholtz transducer source (205 dB re 1 microPa @ 1



Paper number 92JB01706.

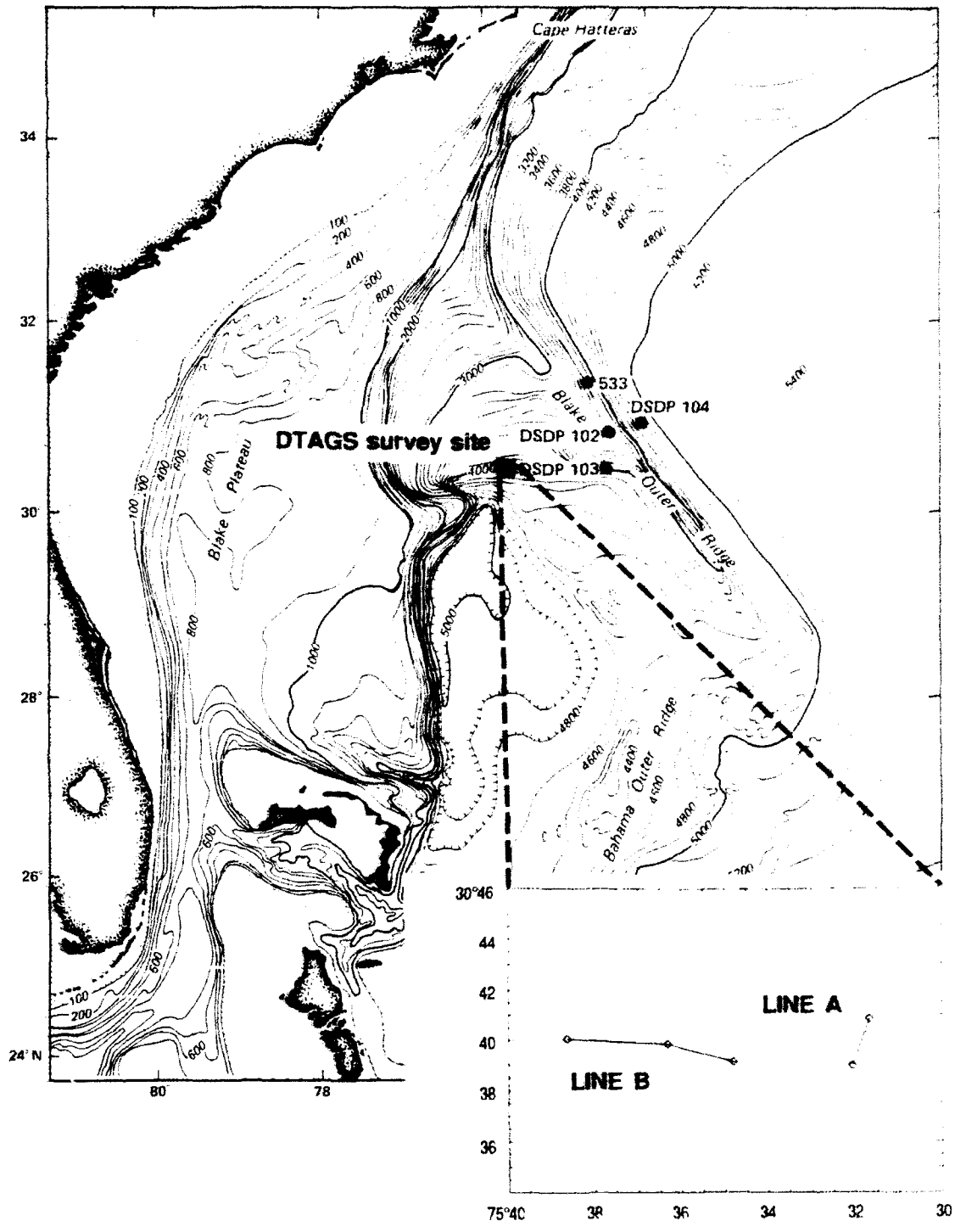


Fig. 1. Map showing relative locations of DTAGS multichannel seismic lines A and B, shown in Figure 3, and DSDP sites. Water depth in the area within the inset is 3600–3800 m.

m) and a linear array containing 24 hydrophone groups. Hydrophone group offsets are from 137 to 620 m with a group separation of 21 m. A single calibrated hydrophone located 57 m from the source records the source reference signature. The source signal, a 125 ms linear chirp from 250–650 Hz, was fired every 30 s, or ~21 m. The data were digitized at 3125 samples/s (0.00032 s/sample). Source and array are towed ~350 m above the seafloor in ocean depths up to 6000 m. Depth sensors at the source and along the array are used to determine array geometry (see *Gettrust et al.* [1988] and *Gettrust and Ross* [1990] for further discussion of the system). Prior to the survey, conductivity-temperature-depth (CTD) measurements were made to obtain estimates of the compressional velocity within the water column over the full water depth; this serves as "ground truth" for water-wave velocity estimates made with DTAGS.

Data processing procedures are similar to those applied to

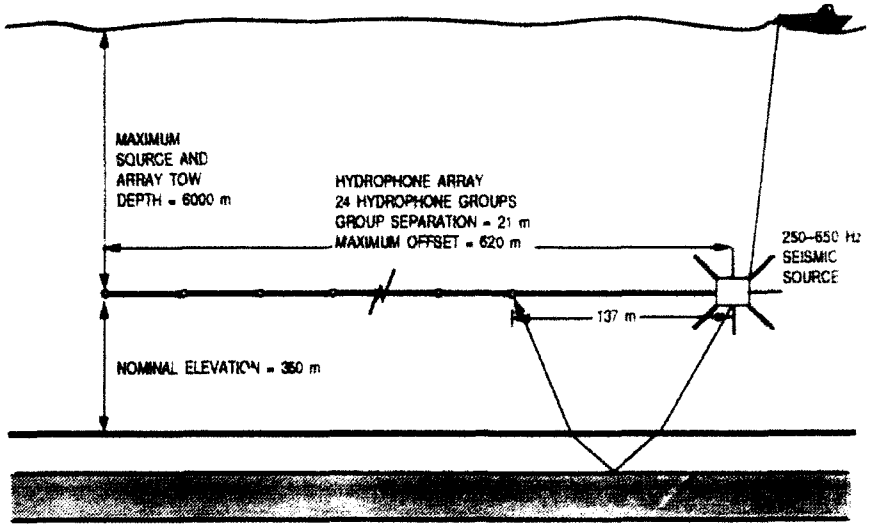


Fig. 2. Deep-Towed Acoustics/Geophysics System geometry when deployed to operating depth, 350–450 m above the sea floor. Digital data are telemetered to the ship via the coaxial tow cable.

standard multichannel seismic data; however, there are differences imposed by the deep-tow techniques used to collect these data. Because array depth is not constrained, a static correction is applied to each channel to place the observations on a datum. As the array tilt is always $<11°$, the maximum time corrections for the array tilt are relatively small (<65 ms).

The ship speed at the slow (~2.0 knots) tow speed required by the DTAGS system is not uniform enough to permit common midpoint (CMP) processing. Therefore all data presented here have been processed in 24-fold common shot point (CSP) format. The use of CSP gathers, gathers made up of all 24 traces from a single shot, will smooth the velocity-depth functions estimated from the data over a ~240-m window at the seafloor. If CMP gathers had been used, lateral resolution of the velocity structure would have been ~21 m as each trace in the gather would contain reflections from the midpoints between the source and receiver.

The data are deconvolved against the signal recorded at the reference hydrophone. It is possible to use the direct water path signals because the deep-tow geometry excludes "ghost" reflections from the water surface from the data window used for these studies.

Static corrections are applied after signal deconvolution to remove the effects of the array tilt. Initial stacking velocity estimates are then made using semblance analysis. The initial stacking velocity, the stacking velocity of the water-sediment interface, is the compressional velocity within the water column. This velocity estimate is compared with (independent) compressional velocity estimates based on direct water-wave travel times to the hydrophone groups and water column compressional velocity obtained from the CTD measurements. The interval velocity estimates for the water column presented here are within 1% of those obtained from the concurrent direct-path measurements and CTD measurements.

Stacking velocity estimates are made using at least every third shot; therefore with a (nominal) 21-m shot separation, estimates are made at 63-m intervals along the profile. Even with this relatively short spatial separation, there are places where lateral heterogeneity requires even finer sampling. In such regions, velocity estimates are made using near-trace (offsets from 137 to 368 m) gathers from consecutive shot gathers (21 m apart), decreasing the amount of lateral smoothing to ~100 m. Velocity estimates are checked using depth sections, created by transforming two-way travel time to depth using these velocity estimates. This is a valuable test, as abrupt changes in horizon depths, inconsistent with the sediment structure shown in the single-channel time section, will occur where velocity estimates are poor. Depth sections also allow us to compare our estimated depth to a major reflection horizon with any coring (e.g., DSDP) data taken near our profiles.

## OBSERVATIONS

Two multichannel seismic lines are presented in this paper. The first, line A, the eastern line in Figure 1, is 2.5 km long and trends from north-south. The second, line B, the western line in Figure 1, is 7.9 km long and trends from west to east. These lines are located approximately 150 km west of DSDP sites 102, 104, and 533, on the southwestern flank of the Blake Outer Ridge. The seismic data are characterized by numerous closely spaced horizontal reflectors extending more than 10 km across the two sections (Figure 3). Similar closely spaced reflectors are observed in conventional multichannel seismic data collected in this area [*Hollister et al.*, 1972; *Dillon et al.*, 1976; *Shipley et al.*, 1979; *Markl and Bryan*, 1983]. The deep-tow data reveal that these closely spaced reflectors are broken by high-angle normal faults less than 1 km apart extending to the maximum depth of the section, approximately 0.65 s below the water-sediment interface (Figures 3 and 4).

Cores recovered at DSDP sites 102, 103, 104, and 533 on the Blake Outer Ridge (Figure 1) consist of uniform hemipelagic silty clay interspersed with thin beds of silty to sandy material to at least 660 m depth [*Hollister et al.*, 1972; *Sheridan et al.*, 1983]. This stratigraphy is the result of fluctuations in the location and strength of the contour

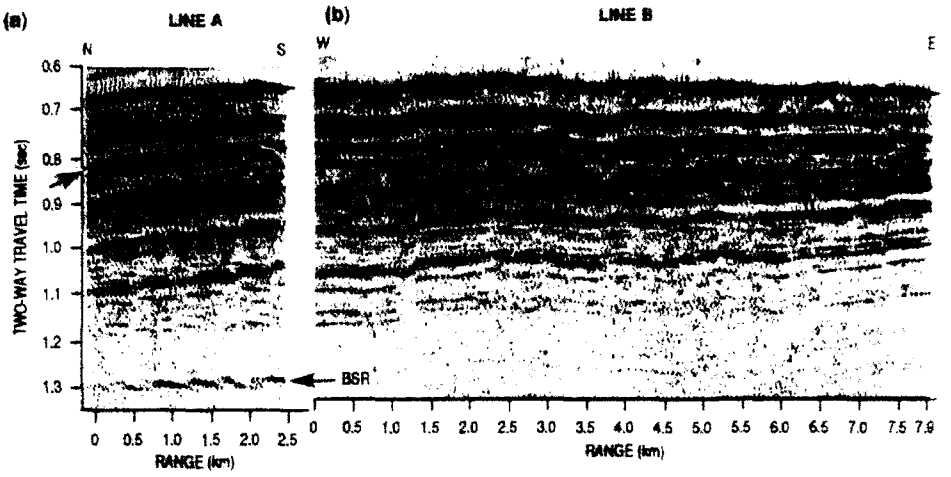


Fig. 3. (*a*) Near-trace single channel seismic section from line A, characterized by thin, closely spaced reflectors and downslope normal faulting. A high-amplitude, shallow reflecting horizon is noted by the arrow on the left-hand side. The arrow on the right-hand side shows the BSR. (*b*) Near-trace single channel seismic section from line B. The laminated reflecting horizons in this section correlated well with the reflectors in line A though the lines are 5 km apart and orthogonal to each other. (Frequency of the reflection data has been reduced for display.)

currents which controlled deposition of these late Miocene to Holocene sediments on the flanks of the Blake Outer Ridge [*Ewing and Hollister*, 1972; *Markl and Bryan*, 1983]. Common offset DTAGS data resolve the small-scale (~5 m vertical, ~21 m horizontal) changes in the sediment structure and reflectivity [*Bowles et al.*, 1991]. The closely spaced acoustic horizons seen in Figure 3 are reflections from the small erosional unconformities [*Markl and Bryan*, 1983] and minor changes in sediment composition and density which are apparent in the core samples.

The water depth where these deep-tow seismic data were recorded ranges from 3660 to 3680 m; this is within the range of water depths at DSDP sites 102, 103, and 104 to the east. As water depth, geologic environment, and sediment type are similar at these DSDP sites and within the DTAGS survey area (Figure 1), the maximum depth of methane hydrate stability at the deep-tow seismic site will be within a few tens of meters of the maximum depth of hydrate stability at DSDP sites 102 and 104; that is, 615–620 m [*Hollister et al.*, 1972].

The strong, continuous BSR at 1.28 to 1.30 s (all travel times presented here are two-way travel times), 0.64 to 0.65 s below the water-sediment interface (Figure 3*a*) appears only in seismic line A (Figure 1). This reflecting horizon has the high-amplitude characteristic of a BSR and occurs at the same arrival time as the BSR observed in seismic sections recorded near DSDP sites 102 and 104, 0.6 s [*Lancelot and Ewing*, 1972]. We show below that the depth of this BSR is ~650 m below the water-sediment interface.

In seismic line B there is no discernable BSR-type reflecting horizon present in the DTAGS multichannel seismic data, though seismic horizons above the BSR observed in the DTAGS data can be correlated exactly from line A, the eastern section, through line B, the western section (Figure 3). A low-amplitude reflection of limited extent may be discerned between 3.5 and 4.5 km, 0.65 s below the water-sediment interface in Figure 3*b*, coincident with the arrival time of the BSR in Figure 3*a*.

Comparison of Figures 3*a* and 3*b* shows that a shallow, high-amplitude acoustic reflector (indicated by the arrow on the left side of Figure 3*a* at 0.83 s) on line A marks the top of a zone of decreased reflectivity relative to the overlying reflectors. This zone of decreased reflectivity extends down to the BSR. Reflectivity does not appear to decrease below this horizon on line B.

On line A, a series of parallel normal faults dipping between 44° and 60° extend from the top of the sediment column down through the BSR, the amount of apparent offset increasing with increasing depth (Figure 4). Fault offsets in the BSR have not been resolved by surface-tow seismic data. The high resolution achievable with DTAGS enables the offsets in the BSR to be clearly imaged in the seismic data.

Progressively larger offset with depth indicates fault slip along these zones of weakness has been occurring contemporaneously with sediment deposition since late Miocene or early Pliocene time. The sense of the faulting, downslope along the ridge flank, is consistent with gravity-driven sliding of the ridge flank sediments. Growth faults like these have been observed on the continental slope to the north [*Carpenter*, 1981; *Dillon et al.*, 1983]. Slope movement along some of the growth faults in these regions is attributed to failure of the sediments along a layer of weak, gas-rich sediments underlying the more rigid methane hydrate layer [*Carpenter*, 1981].

These faults are observed in line B (Figure 3*b*), though they do not exhibit similar, parallel offset since this seismic line is close to parallel to the strike of the fault planes. The strike of the fault planes of these gravity-driven growth faults is nearly parallel to the seafloor contours.

## Seismic Velocity Analysis

Compressional velocity estimates obtained from the eastern and western DTAGS seismic lines show vertical variability as small as a few tens of meters in extent and lateral variability of the order of a hundred meters (Plate 1). In both sections, compressional velocity varies little within the upper 0.18 s below the water-sediment interface, increasing only slightly from the compressional velocity at the sediment

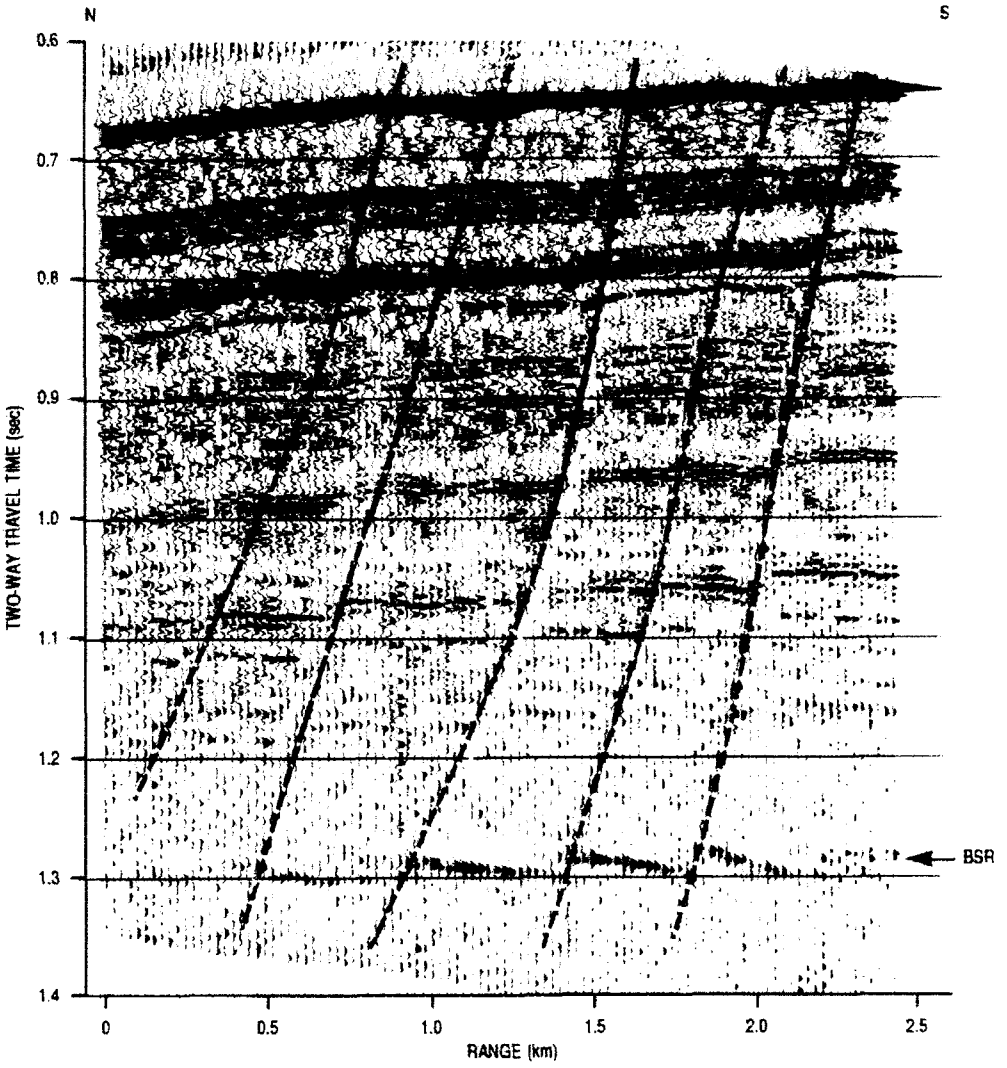


Fig. 4. Near-trace single channel seismic section shown in Figure 3*a* expanded to show parallel normal faults (dipping 44° to 60°) penetrating the BSR. (Frequency of the reflection data has been reduced for display.)

surface, from 1.53 to 1.65 km/s. Impedance contrasts in these sediments are driven by density changes within thin (~1 wavelength) reflecting layers associated with small-scale erosional unconformities [*Markl and Bryan*, 1983]. Large, abrupt changes in compressional velocity across reflecting horizons are not consistent with either our compressional velocity estimates or DSDP velocity data.

At 0.80 to 0.83 s on line A (the top of the zone of low reflectivity) the compressional velocity increases sharply (Plate 1*a*); velocity increases from ~1.65 km/s to >2.00 km/s over 0.09 s. Between this marker horizon (0.20 s below the seafloor) and the BSR (0.60 s below the sediment surface), the compressional velocity increases to 2.4 to 2.7 km/s (Plate 1*a*). Constant velocity normal move-out (NMO) corrected shot gathers (Figure 5) demonstrate the increasing compressional velocity with depth. On line B this steep increase in velocity is not observed continuously across the section though locally, in regions of the order of a hundred meters in extent, there is a steep compressional velocity gradient in which the velocity increases to 2.3 km/s (Plate 1*b*). These high-velocity regions occur within the same depth range as the zones of low reflectivity in line A (Figure 3*a*).

The BSR at the base of line A (Figure 3*a*) is a wide (~0.005 to ~0.010 s) reflecting horizon, indicating that it is composed of reflections from the top and bottom of a layer, having a thickness of the order of one to two wavelengths. Estimates of the compressional velocity within this thin layer cannot be made since a change in NMO corrections between 1.0 and 3.0 km/s at these depths and velocities would be of the order of a single data sample interval. A distinct phase inversion is observed at the top of the BSR, at 1.292 s but not at the lower interface at 1.300 s (Figure 6*a*), indicating that the compressional velocity of the material immediately beneath the upper interface of the BSR is significantly lower than the compressional velocity of the overlying sediment.

Figure 6*b* shows a synthetic seismogram consisting of a shot gather containing traces at the same offsets as shown in Figure 6*a*, 137–242 m. The best fit model was a low-velocity (1.3 km/s) layer ~4-m-thick overlying higher-velocity (2.1 km/s) material (Figure 6*c*). Similar estimates of the velocity and thickness of this thin layer were obtained by *Miller et al.* [1991] for the BSR beneath the inner slope of the Peru-Chile trench.

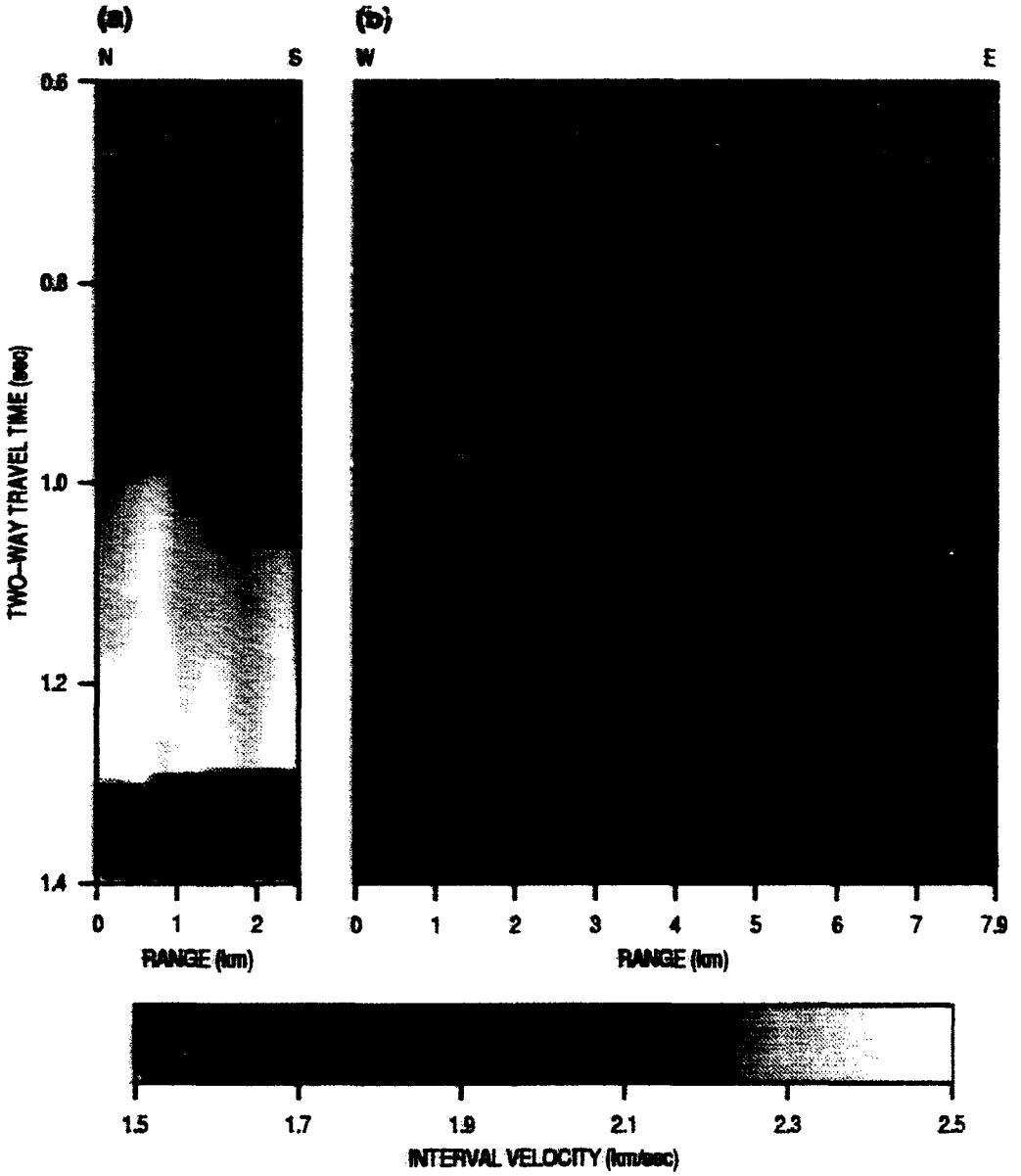


Plate 1. (*a*) Two-dimensional interval velocity model determined from the multichannel data shown in Figure 3*a*. The velocity model extends down to the BSR, at ~1.3 s. (*b*) Two-dimensional interval velocity model derived from the multichannel seismic data shown in Figure 3*b*. Below 1.24 s there are no strong, continuous reflecting horizons for making velocity estimates.

Lateral variability in compressional velocity in line B is as high as 0.3 km/s over distances of the order of 100 m, the minimum lateral smoothing window achievable with these data, (Plate 1*b*). Isovelocity regions as narrow as ~150 m wide exist which the sound velocity remains relatively low, 1.5–1.7 km/s, from the sediment surface to the bottom of the section. Examples of such zones are between 0.9 and 1.05 km and between 2.8 and 3.2 km in Plate 1*b*. These zones are bounded by faults in the seismic sections.

Figures 7*a* and 7*b* are depth sections derived from the data shown in Figures 3*a* and 3*b*, converting from time to depth using the interval velocity functions shown in Plates 1*a* and 1*b*. The closely spaced reflecting horizons above the BSR can be traced from line A through line B, even though the lines are orthogonal and there is considerable lateral variability in the velocity functions. Diffractions from the sharp edges of the faulted horizons have not been migrated. The BSR occurs approximately 650 m below the seafloor and varies in thickness between approximately 3.5 and 7.0 m (assuming the compressional velocity within this low velocity layer is 1.3 km/s). This is consistent with the BSR depth of 615–620 m estimated from drilling results from DSDP sites 102 and 104 [*Hollister et al.*, 1972].

Spatially averaged compressional velocity-depth profiles derived from our data (Figure 8*a*) resolve vertical variability in compressional velocity on a scale of a few tens of meters. These fine-scale velocity changes are not resolved by *Hamilton*'s [1979] empirical compressional velocity-depth function (Figure 8*a*) for the upper 600 m of fine-grained, terrigenous, seafloor sediments. *Hamilton*'s [1979] velocity function predicts a much higher compressional velocity gradient (>1/s) in the upper 100 m of sediment than is obtained from DTAGS

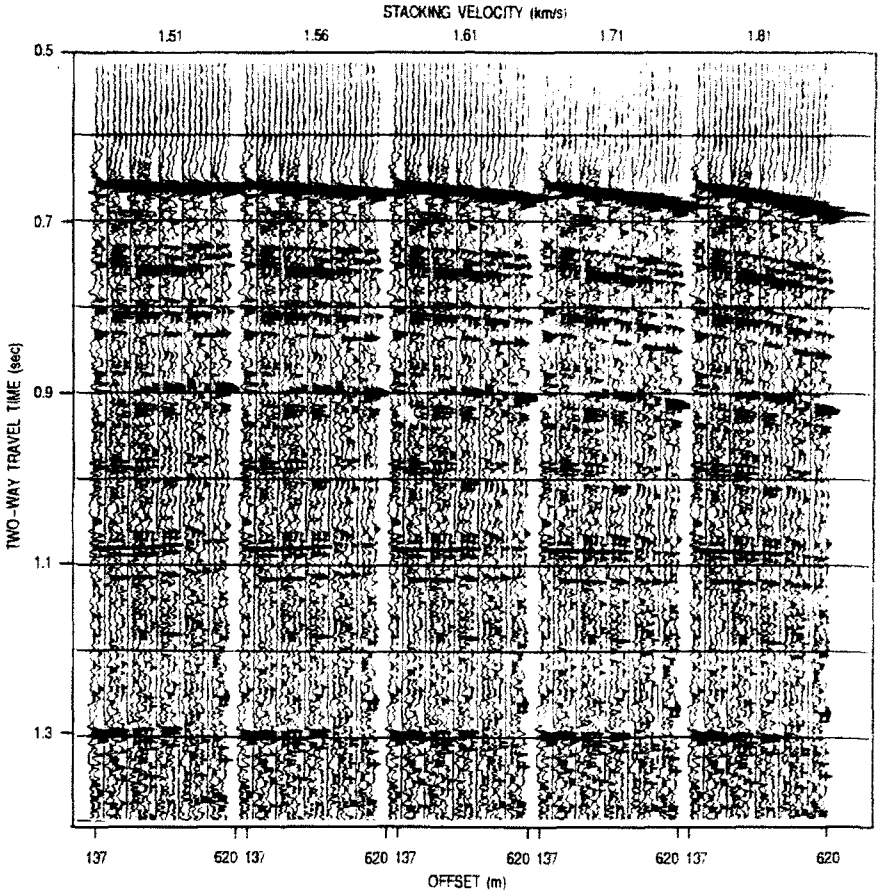


Fig. 5. Sample shot gather from line A (0.95 km, Figure 3*a*), normal move-out (NMO) corrected using the isovelocity functions given above each gather. A given horizon will be horizontal across the gather when NMO corrected using the correct stacking velocity. Horizons below 1.08 s flatten at significantly higher velocities (1.71 to 1.81 km/s) than horizons above 1.00 s. This shows that a steep velocity gradient exists between 1.00 and 1.08 s. (Frequency of the reflection data has been reduced for display.)

data (close to 0/s), even in sediments which do not contain methane hydrate [*Gettrust et al.*, 1988]. The vertical variability in compressional velocity as a function of depth shown by our data is not resolved by the velocity profiles derived from conventional, surface-towed, multichannel seismic data such as the data from the Blake Outer Ridge discussed by *Dillon and Paull* [1983] (Figure 8*b*). This variability is not shown by the compressional velocity profile estimated by relating drilling breaks at DSDP sites 102 and 104 to reflecting horizons in surface-towed single-channel data [*Hollister et al.*, 1972] which is smoothed over hundreds of meters in depth (Figure 8*b*).

## METHANE HYDRATE OCCURRENCE

The two-way travel time to the BSR in the DTAGS data, 0.6 s below the sediment surface, coincides with the two-way travel time to the BSR observed in surface-towed seismic data by *Hollister et al.* [1972], *Tucholke et al.* [1977], and *Shipley et al.* [1979]. The subbottom depth of the BSR in Figure 8*a* correlates with the maximum depth of methane hydrate stability predicted from the phase relation of *Kvenvolden and Barnard* [1983*a*] and *MacLeod* [1982]. This depth also corresponds to the depths at which drilling breaks occurred at DSDP sites 102 and 104.

The geothermal gradient estimated from the depth of the BSR in the DTAGS data, using the relation of *Tucholke et al.* [1977] and sediment density of 1.5 g/cm$^3$ [*Paulus*, 1972] is approximately 3.7°C/100 m. This estimate is close to the 3.6°C/100 m measured value reported by *Kvenvolden and Barnard* [1983*b*] at DSDP site 533 and is within the 3.50° to 3.95°C/100 m range given by *Stoll and Bryan* [1979] as reasonable estimates of the geothermal gradient in sediment containing methane hydrate.

The consistently high (>2.0 km/s) compressional velocity, the decreased reflectivity (used as a diagnostic for estimating hydrate layer thickness by *Dillon et al.* [1991]) between 250 and 650 m depth, and the continuous BSR indicate that methane hydrate forms a thick, continuous layer within the sediment between approximately 250 and 650 m depth below the seafloor in the area covered by line A.

Velocity analysis of the data from the western Blake Outer Ridge line, line B, shows evidence of localized, discontinuous methane hydrate formation even though a distinct BSR is not present in the seismic sections. The homogeneous lithology indicated by the core samples from DSDP sites 102 and 104 [*Hollister et al.*, 1972] is inconsistent with the laterally highly variable compressional velocity and reflectivity. Lateral variability in velocity observed in sediments in which methane hydrate is not present, such as the Bermuda Rise, is significantly lower than that observed here

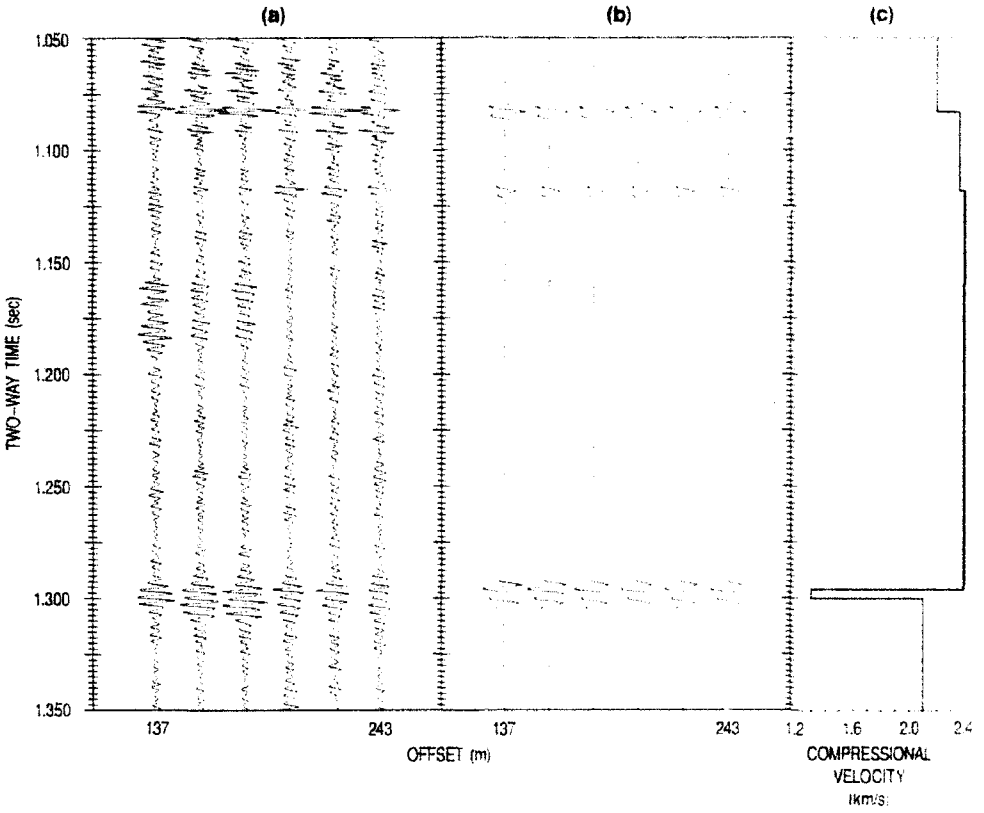


Fig. 6. (*a*) Near-trace shot gather at 1.0 km in line A showing the phase inversion at the top of the BSR (1.29 s). (*b*) Near-trace synthetic seismogram which best fit the gather in Figure 6*a*. This seismogram indicates that the phase is not inverted below the BSR, at 1.30 s. (*c*) Best fit compressional velocity model used to generate the synthetic seismogram in Figure 6*b*.

[*Gettrust et al.*, 1988]. The high lateral variability in sediment compressional velocity observed within the predicted zone of hydrate stability (extending to 650 m subbottom depth) in line B, 1.7 to 2.1 km/s over distances of the order of 100 m, is evidence that regions of methane hydrate-bearing sediments as limited as 100 m in extent coexist with similarly sized regions of sediments containing pore fluid and dissolved methane (if methane is present) but no hydrate. The existence of such regions has been proposed by *Lancelot and Ewing* [1972] and *Galimov and Kvenvolden* [1983].

The localized, discontinuous development of methane hydrate within the sediment may be due to lateral variation

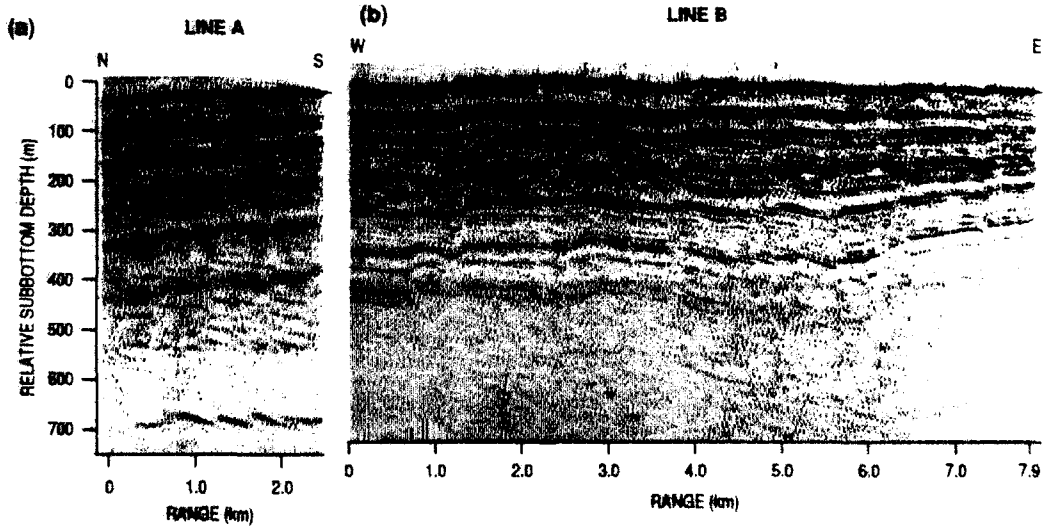


Fig. 7. (*a*) Depth section from line A (Figure 3*a*) converted to depth using the velocity function shown in Plate 1*a*. (b) Depth section from line B (Figure 3*b*) converted to depth using the velocity function shown in Plate 1*b*. (Frequency of the reflection data has been reduced for display.)

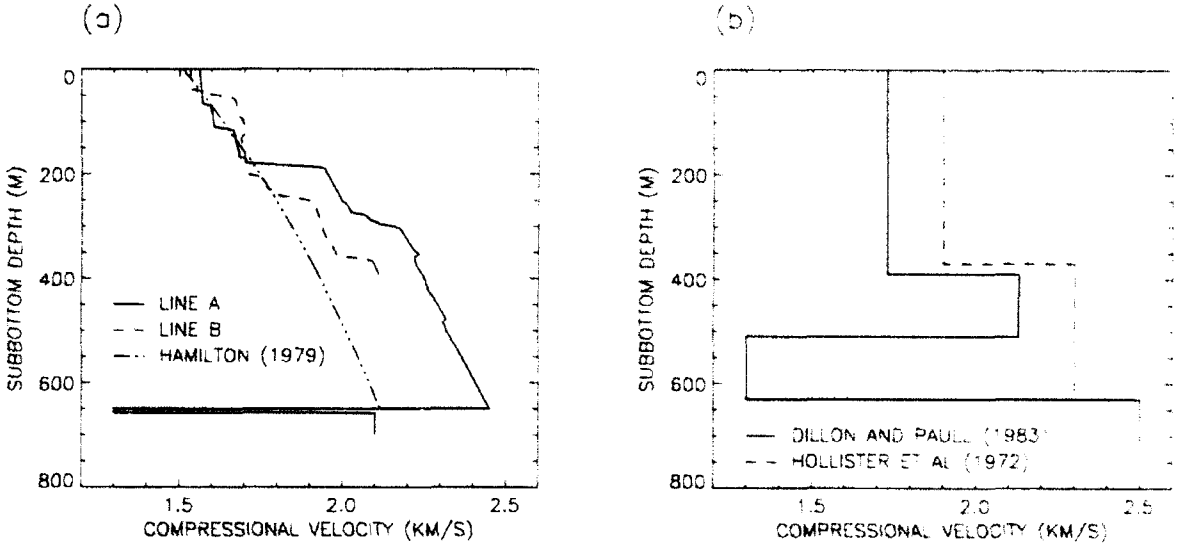


Fig. 8. (*a*) Spatially averaged compressional velocity-depth functions from lines A and B as compared to *Hamilton*'s [1979] empirical compressional velocity-depth curve. Velocity function for line A below the BSR depth (650 m) is based on modeling results. (*b*) Compressional velocity-depth functions obtained from surface-towed multichannel seismic data [*Dillon and Paull*, 1983] and DSDP site 102 and 104 drilling rate data referenced to reflecting horizons in single-channel seismic data [*Hollister et al.*, 1972].

in methane concentration as the gas is generated from organic material in situ [*Brooks et al.*, 1983; *Dillon and Paull*, 1983] or to loss of methane from regions of the sediment which do not presently contain hydrate. Destabilization of the methane hydrate along the fault zones may occur due to the drop in pressure and increase in frictional temperature during rupture. As a result, large quantities of methane may be released from the sediments near the fault zone over a short period of time [*Reed et al.*, 1990]. Between rupture events these faults are barriers to lateral (and vertical) gas migration, preventing hydrate from reforming in the methane-depleted regions within the zone of hydrate stability.

Absence of a high-amplitude, continuous BSR in line B is interpreted to be the result of an overall decrease in the sediment methane concentration between the lines A and B. The sporadic occurrence of methane hydrate inferred from the velocity function shown in Plate 1*b* and the seismic sections from line B (Figures 3*b* and 7*b*) may be characteristic of the transition from a region in which methane hydrate is present in a thick, continuous layer marked by a BSR at the base, as seen in Figure 3*a*, to an area where less methane is present and discontinuous regions containing high concentrations of methane form localized pockets of methane hydrate-bearing sediment.

## NATURE OF THE BSR

Interpretation of the BSR as the equilibrium phase boundary between methane hydrate and methane gas and water appears to conflict with the displacement of the BSR shown in the seismic section in Figure 3. Geochemical evidence suggests that the BSR could be caused by reflection from a dense ankerite or siderite horizon, precipitated as a result of the high concentrations of methane in the pore fluid beneath the methane hydrate phase boundary [*Lancelot and Ewing*, 1972; *Claypool and Kaplan*, 1974; *Matsumoto*, 1989; *Esikov and Pashkina*, 1990]. Thus while related to the location of the maximum depth of stability of methane hydrate, the actual reflecting horizon is caused by the impedance contrast between the dense carbonate formed in situ, such as the "very hard layer or nodule" of ankerite drilled at the depth of the BSR at DSDP site 104 [*Hollister et al.*, 1972], and the overlying gassy hemipelagic marine sediment. This carbonate layer would be offset by faulting but would transgress time horizons within the sediment in the same way as the methane-hydrate phase boundary.

However, the high-amplitude phase inversion at the BSR (Figure 6*a*) is evidence that the impedance difference is caused by a significant decrease in compressional velocity at the BSR rather than a velocity increase. This behavior is consistent with a model in which the BSR is the reflection from the top of a layer of sediment containing methane gas rather than the reflection from a hard layer of carbonate. The coda of the BSR reflection is best modeled (Figure 6*b*) by a thin (~4 m) layer of low compressional velocity (1.3 km/s) sediment at the depth of the BSR overlying sediment with a significantly higher velocity (2.1 km/s) (Figure 6*c*). Thickening of the BSR updip along the faulted sections (Figure 4) may be due to migration of the free gas upward along the base of the impermeable hydrate.

The thin, gas-rich layer below the BSR, suggested by the model, would have low shear strength, providing a surface along which slope failure may occur. Growth faults, like those seen in line A (Figure 4), are characteristic of slope failure along a deeper, less rigid sediment layer. *Dillon et al.* [1983] observed such faulting in which the less rigid layer was salt. *Carpenter* [1981] observed these growth faults in which failure occurred along a layer of gas-rich sediment. Dissociation of the hydrate at the base of the BSR, due to small pressure or temperature changes, may facilitate slip along this zone of weakness [*Paull et al.*, 1991; *Dillon*, 1991].

Distinct offsets in the equilibrium phase boundary marked by the BSR are consistent with the discontinuity in the compressional stress field across the fault zone [*Hafner*,

1951]. The increase in depth to the BSR suggests pressure is higher at the BSR depth on the downthrown side of the fault relative to the upthrown side. Higher pressure on the downthrown sides of these faults is consistent with the observed displacement along these growth faults [*Hafner*, 1951]. The pressure increase across the fault from the upthrown side to the downthrown side may abruptly increase the maximum depth of methane hydrate stability as much as ~20 m at the fault zone. This pressure effect would decrease with increasing distance from the fault, causing the depth to the BSR in this case to decrease to the south between the faults (Figure 4).

Given the water depth (~3700 m) and depth to the BSR (~650 m) in the area studied, the phase diagram of *Kvenvolden and Barnard* [1983*a*, Figure 1], indicates that a change in pressure across a fault of ~200 kPa (~2 bars) would be consistent with a BSR displacement of 15–20 m. This differential stress is within the bounds of the shear strength of saturated clays at these depths [*Craig*, 1983, p. 135].

## CONCLUSIONS

Evidence from deep-towed multichannel seismic data (compressional velocity structure, variability in reflectivity, phase inversions at the BSR) shows that methane hydrate may occur continuously within a ~400-m-thick layer of sediment extending down to the maximum depth of hydrate stability, characterized by low reflectivity and underlain by a BSR, or it may be limited to regions on the order of a 100 m in extent where high concentrations of methane exist in discontinuous patches. Patchy development of methane hydrate may be due to loss of methane from the sediment or to a decrease in the amount of methane generated in situ.

Velocities of the order of 2.5 km/s may be accounted for by lithologic changes within the sediment such as the development of dense carbonate or chert layers. However, the uniform lithology of the Blake Outer Ridge sediments between the water-sediment interface and depths exceeding 600 m, as shown by the cores from DSDP sites 102, 103, and 104, and the continuous nature of the reflecting horizons extending 8 km across line A to line B, 5 km away, do not support lithologic changes as the cause of the anomalous high velocities in either the eastern or the western sections.

These high-resolution data show that the BSR has finite thickness of 5–10 m. The phase inversion at the top of the BSR shows that this 5- to 10-m-thick layer is a low-velocity zone (most likely free gas bearing) which also is a zone of weakness that may be causally related to the normal faults observed penetrating the BSR. The ~20-m fault offset resolved with these data along the BSR is not resolved in surface-towed seismic data. As noted previously, this offset is consistent with a reasonable estimate of the pressure differential across the fault. If there is surficial expression of these faults that can be resolved with side scan sonar images, side scan sonar mapping of methane hydrate regions could serve as a rapid means of refining estimates of the areal extent of these zones; this, in combination with additional high-resolution multichannel seismic data, would provide additional insight into the volume of methane hydrate existing in the marine environment. Although only two-dimensional profiles were taken during the experiment discussed here, the ability to resolve methane hydrate zones within deep-ocean sediments (as demonstrated with these data) indicates that it will be possible to use high-resolution multichannel seismic data in the future to obtain viable in situ estimates of the volume of methane hydrate and hence the importance of these features in terms of energy sources and their potential impact on the greenhouse effect [*Paull et al.*, 1991].

*Acknowledgments.* The authors thank the reviewers for their many helpful suggestions. We also thank Dennis Lindwall for his assistance in modeling the seismic data. This work was supported by the Office of Naval Technology, program element 0602435N, and the Office of Naval Research, program element 0601153N. NOARL contribution JA 362:072:91.

## REFERENCES

Baker, P. E., Experiments on hydrocarbon gas hydrates in unconsolidated sand, in *Natural Gases in Marine Sediments*, edited by I. R. Kaplan, pp. 227–234, Plenum, New York, 1974.

Bowles, F. A., J. F. Gettrust, and M. Rowe, Geological interpretations based on deep-tow single channel and multichannel seismic data from the Bermuda Rise, *Marine Geology*, *96*, 279–293, 1991.

Brooks, J. M., L. A. Barnard, D. A. Wiesenburg, and M. C. Kennicutt II, Molecular and isotopic compositions of hydrocarbons at site 533, Deep Sea Drilling Project leg 76, in *Initial Reports of the Deep Sea Drilling Project*, *76*, edited by R. E. Sheridan, F. M. Gradstein, et al., pp. 377–389, U.S. Government Printing Office, Washington, D. C., 1983.

Bryan, G. M., In situ indications of gas hydrate, in *Natural Gases in Marine Sediments*, edited by I. R. Kaplan, pp. 299–308, Plenum, New York, 1974.

Carpenter, G., Coincident sediment slump/clathrate complexes on the U.S. Atlantic continental slope, *Geo Mar. Lett.*, *1*, 29–32, 1981.

Claypool, G. E., and I. R. Kaplan, The origin and distribution of methane in marine sediments, in *Natural Gases in Marine Sediments*, edited by I. R. Kaplan, pp. 99–140, Plenum, New York, 1974.

Craig, R. F., *Soil Mechanics*, 3rd ed., pp. 135, Van Nostrand Reinhold, New York, 1983.

Dillon, W. P., Overview of the National Workshop on Gas Hydrates, in *Report on National Workshop on Gas Hydrates*, DOE/METC - 91/6/24, DE 91016654, pp. 3–7, U.S. Department of Energy, Morgantown, W. V., 1991.

Dillon, W. P., and C. K. Paull, Marine gas hydrates, II, Geophysical evidence, in *Natural Gas Hydrates: Properties, Occurrence and Recovery*, edited by John L. Cox, pp. 73–90, Butterworth, Stoneham, Mass., 1983.

Dillon, W. P., R. E. Sheridan, and J. P. Fail, Structure of the western Blake-Bahama basin as shown by 24-channel CDP profiling, *Geology*, *4*, 459–462, 1976.

Dillon, W. P., J. A. Grow, and C. K. Paull, Unconventional gas hydrates seals may trap gas off southeast U.S., *Oil and Gas J.*, *78*, 124–130, 1980.

Dillon, W. P., P. Popenoe, J. A. Grow, K. D. Klitgord, B. A. Swift, C. K. Paull, and K. V. Cashman, Growth faulting and salt diapirism: Their relationship and control in the Carolina Trough, eastern North America, in *Studies in Continental Margin Geology*, *AAPG Mem. 34*, edited by J. S. Watkins and C. L. Drake, pp. 21–46, 1983.

Dillon, W. P., M. W. Lee, K. Fehlhaber, and D. R. Hutchinson, Estimation of amounts of gas hydrate in marine sediments using amplitude reduction of seismic reflections, paper presented at Acoustical Society of America 121 Meeting, Baltimore, April 29 to May 3, 1991.

Esikov, A. D., and V. I. Pashkina, A study of the process of joint formation of methane gas-hydrate and authigenic carbonates in bottom sediments in the Sea of Okhotsk, *Nucl. Geophys.*, *4*, 135–141, 1990.

Ewing, J. I., and C. H. Hollister, Regional aspects of deep sea drilling in the western North Atlantic, in *Initial Reports of the Deep Sea Drilling Project, 11*, edited by C. D. Hollister, J. I.

Ewing, et al., pp. 951–972. U.S. Government Printing Office, Washington, D. C., 1972.

Galimov, E. M., and K. A. Kvenvolden, Concentrations and carbon isotopic compositions of CH4 and CO2 in gas from sediments of the Blake Outer Ridge, Deep Sea Drilling Project leg 76, in *Initial Reports of the Deep Sea Drilling Project, 76*, edited by R. E. Sheridan, F. M. Gradstein, et al., pp. 403–407, U.S. Government Printing Office, Washington, D. C., 1983.

Gettrust, J. F. and J. H. Ross, Development of a low-frequency, deep-towed geoacoustics system, *Proc. Oceans '90*, 38–40, 1990.

Gettrust, J. F., M. Grimm, S. Madosik, and M. Rowe, Results of a deep-tow multichannel survey on the Bermuda Rise, *Geophys. Res. Lett., 15*, 1413–1416, 1988.

Hafner, W., Stress distributions and faulting, *Geol. Soc. Am. Bull., 62*, 373–398, 1951.

Hamilton, E. L., Vp/Vs and Poissons's ratios in marine sediments and rocks, *J. Acoust. Soc. Am., 66*, 1093–1101, 1979.

Hollister, C. D., J. I. Ewing, D. Habib, J. C. Hathaway, Y. Lancelot, H. Luterbacher, F. J. Paulus, C. W. Poag, J. A. Wilcoxon, P. Worstell, Sites 102-103-104 - Blake-Bahama Outer Ridge (northern end), in *Initial Reports of the Deep Sea Drilling Project, 11*, edited by C. D. Hollister, J. I. Ewing, et al., pp. 135–143, U.S. Government Printing Office, Washington, D. C., 1972.

Kvenvolden, K. A., and L. A. Barnard, Hydrates of natural gas in continental margins, in *Studies in Continental Margin Geology, AAPG Mem. 34*, edited by J. S. Watkins and C. L. Drake, pp. 631–640, American Association of Petroleum Geologists, Tulsa, Oklahoma, 1983*a*.

Kvenvolden, K. A., and L. A. Barnard, Gas hydrates of the Blake Outer Ridge, site 533, Deep Sea Drilling Project leg 76, in *Initial Reports of the Deep Sea Drilling Project, 76*, edited by R. E. Sheridan, F. M. Gradstein, et al., pp. 353–365, U.S. Government Printing Office, Washington, D. C., 1983*b*.

Kvenvolden, K. A., and T. J. McDonald, Gas hydrates of the Middle America trench - Deep Sea Drilling Project leg 84, in *Initial Reports of the Deep Sea Drilling Project*, vol. 84, edited by R. von Huene, J. Aubouin, et al., pp. 667–681, U.S. Government Printing Office, Washington, D. C., 1985.

Lancelot, Y., and J. I. Ewing, Correlation of natural gas zonation and carbonate diagenesis in Tertiary sediments from the northwest Atlantic, in *Initial Reports of the Deep Sea Drilling Project, 11*, edited by C. D. Hollister, J. I. Ewing, et al., pp. 791–799, U.S. Government Printing Office, Washington, D. C., 1972.

MacLeod, M. K., Gas hydrates in ocean bottom sediments, *Am. Assoc. Petr. Geol. Bull., 66*, 2649–2662, 1982.

Markl, R. G., and G. M. Bryan, Stratigraphic evolution of Blake Outer Ridge, *Am. Assoc. Pet. Geol. Bull., 67*, 666–683, 1983.

Mathews, M. A., and R. von Huene, Site 570 methane hydrate zone, in *Initial Reports of the Deep Sea Drilling Project*, vol. 84, edited by R. von Huene, J. Aubouin, et al., pp. 773–790, U.S. Government Printing Office, Washington, D. C., 1985.

Matsumoto, R., Isotopically heavy oxygen-containing siderite derived from the decomposition of methane hydrate, *Geology, 17*, 707–710, 1989.

McIver, R. D., Hydrocarbon gas (methane) in canned deep sea drilling project core samples, in *Natural Gases in Marine Sediments*, edited by I. R. Kaplan, pp. 63–70, Plenum, New York, 1974.

Miller, J. J., M. W. Lee, and R. von Huene, An analysis of a seismic reflection from the base of a gas hydrate zone, offshore Peru, *Am. Assoc. Pet. Geol. Bull., 75*, 910–924, 1991.

Paull, C. K. and W. P. Dillon, Appearance and distribution of the gas-hydrate reflection in the Blake Ridge region, offshore southeastern United States, *Misc. Field Stud. Map MF-1252*, U.S. Geological Survey, Washington, D. C., 1981.

Paull, C. K., W. U. Ussler III, and W. P. Dillon, Is the extent of glaciation limited by marine gas-hydrates?, *Geophys. Res. Lett., 18*, 432–434, 1991.

Paulus, F. J., Leg 11 measurements of physical properties in sediments of the western North Atlantic and their relationship to sediment consolidation, in *Initial Reports of the Deep Sea Drilling Project*, vol. 11, edited by C. D. Hollister, J. I. Ewing, et al., pp. 667–722, U.S. Government Printing Office, Washington, D. C., 1972.

Reed, D. L., E. A. Silver, J. E. Tagudin, T. H. Shipley, and P. Vrolijk, Relations between mud volcanoes thrust deformation, slope sedimentation, and gas hydrate, offshore north Panama, *Mar. Pet. Geol., 7*, 44–54, 1990.

Sheridan, R. E., et al., Site 533, Blake Outer Ridge, in *Initial Reports of the Deep Sea Drilling Project*, vol. 76, edited by R. E. Sheridan, F. M. Gradstein, et al., pp. 35–140, U.S. Government Printing Office, Washington, D. C., 1983.

Shipley, T. H., M. H. Houston, R. T. Buffler, F. J. Shaub, K. J. McMillen, J. W. Ladd, and J. L. Worzel, Seismic evidence for widespread possible gas hydrate horizons on continental slopes and rises, *Am. Assoc. Pet. Geol. Bull., 63*, 2204–2213, 1979.

Sloan, E. D., *Clathrate Hydrates of Natural Gases*, 641 pp., Marcel Dekker, New York, 1990.

Stoll, R. D., and G. M. Bryan, Physical properties of sediments containing gas hydrates, *J. Geophys. Res., 84*, 1629–1634, 1979.

Stoll, R. D., J. Ewing, and G. M. Bryan, Anomalous wave velocities in sediments containing gas hydrates, *J. Geophys. Res., 76*, 2090–2094, 1971.

Tucholke, B. E., G. M. Bryan, and J. I. Ewing, Gas-hydrate horizons detected in seismic-profile data from the western North Atlantic, *Am. Assoc. Pet. Geol. Bull., 61*, 698–707, 1977.

J. F. Gettrust and M. M. Rowe, NRL Code 362, Building 1005, Stennis Space Center, MS 39529.

(Received January 20, 1992;
revised June 15, 1992;
accepted July 15, 1992.)